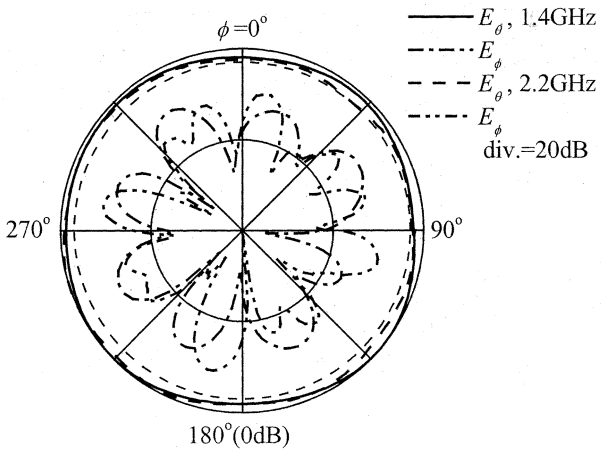

Fig. 4. Measured and simulated radiation patterns at 1.4 and 2.2 GHz in $\phi = 90°$.

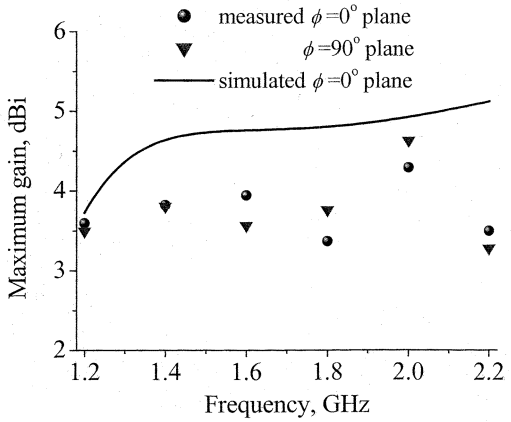

Fig. 5. A comparison of measured and simulated maximum gains.

IV. Conclusion

A new roll monopole antenna has been presented for broadband applications experimentally and numerically. As known, a planar monopole usually features a broad impedance bandwidth due to the larger size of its radiator and the coupling between the ground plane and the bottom edge of the radiator. The almost symmetrical structure of the roll monopole has significantly improved the radiation performances of the broadband monopole within a remarkably broad bandwidth.

References

[1] H. Kawakami and G. Sato, "Broadband characteristics of rotationally symmetric antennas and thin wire constructs," *IEEE Trans. Antennas Propagat.*, vol. AP-35, pp. 26–32, Jan. 1987.

[2] H. Nakano, N. Ikeda, Y. Wu, R. Suzuki, H. Mimaki, and J. Yamauchi, "Realization of dual-frequency and wide-band VSWR performances using normal helical and inverted-F antennas," *IEEE Trans. Antennas Propagat.*, vol. 46, pp. 788–793, June 1998.

[3] S. D. Rogers and C. M. Butler, "Cage antennas optimized for bandwidth," *Electron. Lett.*, vol. 36, no. 11, pp. 932–933, 2000.

[4] W. Cho, M. Kanda, H. Hwang, and M. W. Howard, "A disk-loaded thick cylindrical dipole antenna for validation of an EMC test site from 30 to 300 MHz," *IEEE Trans. Electromagn. Compat.*, vol. 42, pp. 172–180, May 2000.

[5] G. H. Brown and O. M. Woodward Jr., "Experimentally determined radiation characteristics of conical and triangular antennas," *RCA Rev.*, vol. 13, no. 4, pp. 425–452, Dec. 1952.

[6] S. Honda, M. Ito, H. Seki, and Y. Jinbo, "A disk monopole antenna with 1:8 impedance bandwidth and omnidirectional radiation pattern," in *Proc. ISAP'92*, Sapporo, Japan, 1992, pp. 1145–1148.

[7] N. P. Agrawall, G. Kumar, and K. P. Ray, "Wide-band planar monopole antenna," *IEEE Trans. Antennas Propagat.*, vol. 46, pp. 294–295, Feb. 1998.

[8] M. J. Ammann, "Square planar monopole antenna," in *Proc. Nat. Conf. Antennas Propagat.*, York, England, 1999, pp. 37–40.

[9] Z. N. Chen, "Impedance characteristics of planar bow-tie-like monopole antennas," *Electron. Lett.*, vol. 36, no. 13, pp. 1100–1101, 2000.

Figure of Merit for Multiband Antennas

Juan M. Rius, María C. Santos, and Josep Parrón

***Abstract*—This communication defines a figure of merit for multiband antennas that gives an objective quantification of the similarities between radiation patterns at the different antenna operating bands.**

***Index Terms*—Antenna radiation pattern, multiband antennas.**

I. Introduction

In recent years, great interest has arisen in multiband prefractal antennas [1]–[3], whose multiband behavior with respect to the similarity of radiation patterns at the different resonant bands apparently outperforms that of classical multiband antennas [4]. However, very often the radiation patterns at the different operating frequency bands are compared only by mere visual inspection of planar cuts over the principal planes. A more rigorous and objective means of comparison between radiation patterns in the whole three–dimensional (3-D) space is found of interest.

In this communication, we propose an objective criterion to establish if two radiation patterns can, or cannot, be considered similar. The key is a reference tolerance table, which sets the maximum radiation level difference in decibels (dB) between the two patterns that is acceptable for each radiation pattern level. Simple surface integrals over the unity radius sphere produce a numerical value, which constitutes a measure of the similarity between the two patterns in the whole 3-D space. The figure of merit thus defined can be easily matched to the specific requirements of different applications by the definition of reference tolerance tables tailored to each application. This procedure should provide a framework of reference to compare patterns at different bands and assess the behavior of multiband antennas.

Manuscript received July 26, 2002; revised November 20, 2002. This work was supported in part by the Departament d'Universitats Recerca i Societat de la Informació (DURSI) of the Generalitat de Catalunya under Distinció de la Generalitat de Catalunya per a la Promoció de la Recerca Universitaria, the Spanish Comisión Interministerial de Ciencia y Tecnología (CICYT) through Grants TIC 2001-2364-C01-01 and TIC 2000-0996 and in part by the European Commission through FET project IST-2001-33055.

The authors are with Department of Signal Theory and Communications (TSC), Universitat Politècnica de Catalunya (UPC), Barcelona 08035, Spain.

Digital Object Identifier 10.1109/TAP.2003.818793

TABLE I
EXAMPLE OF A VERY RESTRICTIVE REFERENCE TOLERANCES TABLE

Absolute level	-50	-40	-30	-20	-10	-5	0
Tolerance (dB)	-50	-30	-10	-5	-3	-2	-1

TABLE II
EXAMPLE OF A TABLE WITH MORE RELAXED TOLERANCES

Absolute level	-50	-40	-30	-20	-10	-5	0
Tolerance (dB)	-50	-37.5	-25	-15	-7	-4	-2

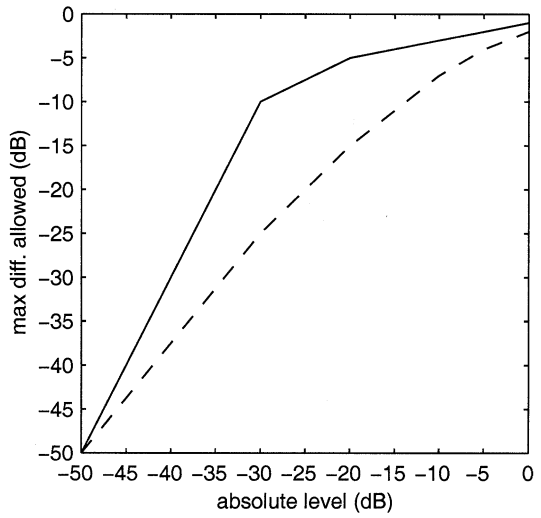

Fig. 1. Maximum acceptable decibels difference between two radiation patterns plotted for each normalized radiation pattern level in decibels. Continuous line: Table I, dotted line: Table II.

II. FIGURE OF MERIT

When defining a figure of merit that should provide a measure of the degree of similarity between two radiation patterns, one has to bear in mind that the numerical value obtained must show a correspondence to what it is commonly and in practice understood as similar. On the other hand, it needs to provide a sufficient dynamic margin that allows ranking of similar and nonsimilar patterns in a common reference framework, and assign significantly different numbers to those pairs of patterns which, from a practical point of view, present significantly different degrees of similarity. Finally, it is important to define it in a simple as well as intuitive manner, so that its numerical value can be easily and quickly calculated and its physical meaning directly understood.

In most applications of multiband antennas, one generally assumes that two radiation patterns are similar if their absolute difference in dB into each space direction is below a threshold, which sets the similarity tolerance. In practice this threshold or similarity tolerance is not constant over the whole space, but rather it is dependent on the radiation pattern level, compared to the maximum, found into each space direction. To account for this, the figure of merit is computed in basis of a tolerance table, which assigns a tolerance value in dB to each radiation pattern level.

Tables I and II are examples of specification of a reference tolerance table. The radiation pattern levels are normalized to 0 dB in the maximum. Linear interpolation is assumed for values not explicitly given in the table. Both tolerance tables are represented graphically in Fig. 1. Table I is very restrictive and therefore should differentiate between patterns that are found similar if the less restrictive Table II is used.

Commonly, different tolerance tables will be used for different fields of application. In any case, when comparing the different usable patterns of a multiband antenna, the reference tolerance table must be always specified together with the figure of merit.

We propose here a figure of merit formula that gives values between zero and one as follows: If all space directions fulfill the condition for similarity given by the reference tolerance table, i.e., throughout the whole space the absolute difference between the radiation levels is kept below the corresponding tolerance value, the figure of merit must reach its maximum value (one). In the opposite case, the figure of merit is equal to the minimum value (zero). If only part of the space directions in the 3-D radiation pattern fulfill the condition, the figure of merit takes an intermediate value equal to the fraction of surface area over a unity radius sphere where the absolute difference in dB between the two radiation patterns does not exceed the corresponding threshold for similarity given by the reference tolerance table:

$$S = \frac{\text{Surface area below tolerance}}{\text{Total area}}. \tag{1}$$

Given two normalized radiation patterns $D_1(\theta,\varphi)$ and $D_2(\theta,\varphi)$, with θ and φ, respectively, the spherical elevation and azimuth angles and the pattern values expressed in dB, the figure of merit (1) is computed as

$$S = \frac{1}{4\pi}\int_0^{2\pi}\int_0^{\pi} F(\theta,\varphi)\sin(\theta)\,d\theta\,d\varphi \tag{2}$$

being the $F(\theta,\varphi)$ function given by

$$F(\theta,\varphi) = \begin{Bmatrix} 1, & if\ \alpha(\theta,\varphi) < 1 \\ 0, & \text{otherwise} \end{Bmatrix} \tag{3}$$

with

$$\alpha(\theta,\varphi) = \left| \frac{|D_1(\theta,\varphi)| - |D_2(\theta,\varphi)|}{|\text{tol}\,(\max\,(D_1(\theta,\varphi), D_2(\theta,\varphi)))|} \right| \tag{4}$$

where $\text{tol}(\max(D_1(\theta,\varphi), D_2(\theta,\varphi)))$ denotes the tolerance (in dB) corresponding to the highest of $D_1(\theta,\varphi)$ and $D_2(\theta,\varphi)$. This results in a worst case scenario with respect to the patterns D_1 and D_2.

Thus defined, the figure of merit S takes values $0 < S < 1$ with $S = 1$ for completely similar patterns (not necessarily identical but with level differences in dB that at every space point do not exceed the corresponding dB tolerance) and $S = 0$ for total absence of similarity.

A. Weighted Figure of Merit

The above definition should prove useful for the majority of applications where emphasis is in deciding whether two antenna patterns can or cannot be considered similar for a particular application, that is, according to a particular reference tolerance table. However, the fact that all space directions with absolute level differences below the tolerance value are assigned the same contribution to the surface integral regardless of the actual value of the absolute level difference, can render very difficult to discriminate among pairs of patterns with close similarity properties.

Fine tuning of the degree of similarity is accomplished by weighting the contribution of each space direction with absolute level difference below the tolerance value according to the actual absolute level difference encountered. This leads to an alternative formulation of the figure of merit $F(\theta,\varphi)$ given by

$$F_w(\theta,\varphi) = \begin{Bmatrix} 1-\alpha(\theta,\varphi), & \text{if } \alpha(\theta,\varphi) < 1 \\ 0, & \text{otherwise} \end{Bmatrix} \tag{5}$$

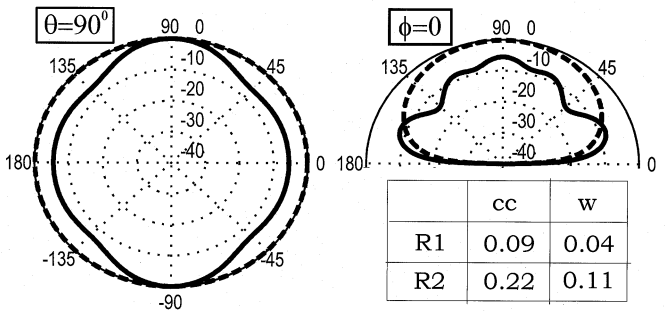

	cc	w
R1	0.09	0.04
R2	0.22	0.11

Fig. 2. Radiation pattern cuts obtained through numerical simulation for a log-periodic multiband antenna, and table containing the values of the figure of merit according to the definitions given in the text. Continuous line: third operative band, dotted line: first operative band.

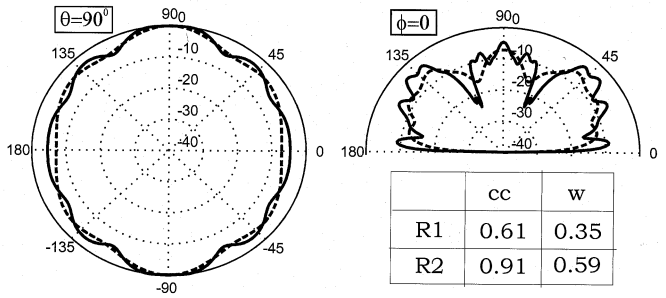

	cc	w
R1	0.61	0.35
R2	0.91	0.59

Fig. 3. Radiation patterns of the fifth (continuous line) and the fourth (dotted line) operative bands of the same antenna as in Fig. 2.

where subscript w stands for weighted. Note that in the case of weighted figure of merit, $S = 1$ is assigned only to completely identical patterns.

III. Results

This section illustrates the application of the above two definitions of the figure of merit through representative examples. Extensive tests have been performed comparing a broad variety of radiation patterns that confirm the consistency of the definitions (2), (3), and (5) for the figure of merit and prove it useful to give a measure of the degree of similarity observed. A few representative cases are presented in Figs. 2 to 6, showing the cuts over two principal planes, $\theta = 90^\circ$ and $\varphi = 0$, of the two radiation patterns being compared, along with a table containing the numerical values found for the figure of merit. Two different reference tolerance tables have been used, given in Tables I and II above and, respectively, labeled R1 and R2. The figure of merit computed with the first formula (3) is labeled constant contribution cc, and the weighted figure of merit (5) is labeled w. The radiation patterns shown in Figs. 2 to 4 have been obtained by numerical simulation of two different multiband antennas using the Method of Moments [5], while the patterns in Figs. 5 and 6 result from a mathematical formula. The first example (Figs. 2 and 3) is a five-band log-periodic antenna called parany and described in [1]. The second one is a five-band Sierpinski prefractal monopole.

Figs. 2 and 3 show the pairs of radiation patterns of the parany antenna at different operating bands that, according to our definitions of the figure of merit, give respectively the poorest and the best similarity values, thus providing some insight into the margin of figure of merit values that can be obtained for that particular antenna. They correspond, respectively, to the first and third (Fig. 2) and to the fourth and fifth (Fig. 3) operative bands.

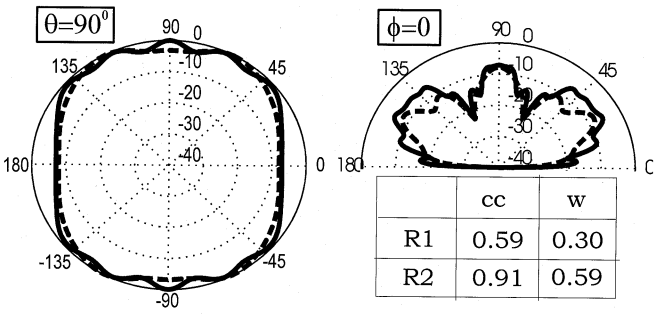

	cc	w
R1	0.59	0.30
R2	0.91	0.59

Fig. 4. Same as Fig. 3 but for a Sierpinski prefractal multiband antenna.

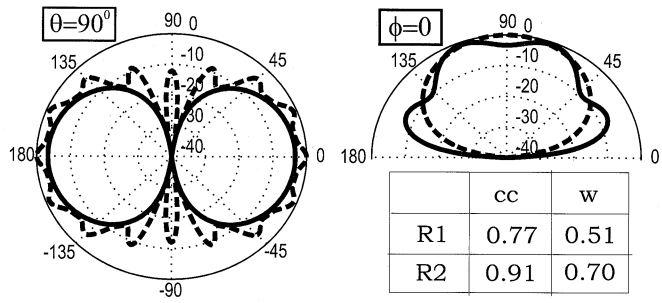

	cc	w
R1	0.77	0.51
R2	0.91	0.70

Fig. 5. Same as Fig. 2 with the radiation patterns obtained through mathematical formulation. Continuous line: $a\sin^2(\theta)\cos^2(\phi) + (1 - a)\sin^2(4\theta)\cos^4(8\phi)$, $a = 0.68$, dotted line: $b\sin^2(\theta)\cos^2(\phi) + (1 - b)\sin^2(\theta)\cos^4(8\phi)$, $b = 0.75$.

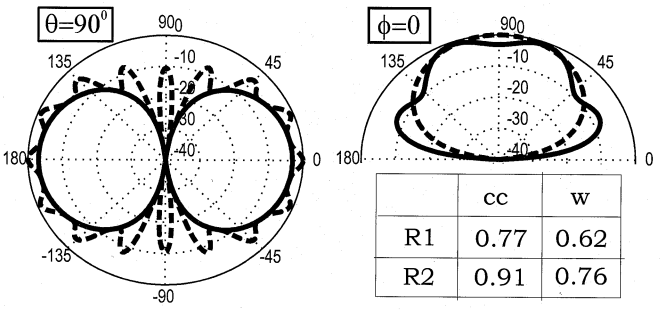

	cc	w
R1	0.77	0.62
R2	0.91	0.76

Fig. 6. Same as Fig. 5 with $a = b = 0.7$.

Fig. 4 compares the radiation patterns for the fourth and fifth operative bands for the Sierpinski antenna. It is remarkable that only the weighted figure of merit (5) with the more restrictive tolerance table, R1, is able to decide that the first multiband antenna in Fig. 3 has patterns more similar than the second antenna in Fig. 4.

Finally, the two pairs of patterns shown in Figs. 5 and 6, obtained through mathematical functions, illustrate how the use of the weighted figure of merit (5) can help to decide between pairs of patterns that look very similar. In the case shown, the patterns in Fig. 6 are found more similar than the patterns in Fig. 5.

IV. Conclusion

A figure of merit that objectively quantifies the similarity between two given radiation patterns has been defined. A reference tolerance table defines the maximum acceptable differences in dB between the patterns. The tolerance table can be tailored to each application. The computation of the figure of merit involves a surface integration in the whole space to account for the full 3-D radiation pattern. Consistency

and usefulness of the definitions has been proved through examples of application.

The adoption of this figure of merit as a standard would provide a useful tool to compare and assess the behavior of multiband antennas.

REFERENCES

[1] C. Puente, "Fractal Antennas," Doctorate thesis, Universitat Politècnica de Catalunya, 1997.

[2] C. Puente, J. Romeu, R. Pous, X. García, and F. Benitez, "Fractal multiband antenna based on the Sierpinski gasket," *IEE Electron. Lett.*, vol. 32, pp. 1–2, Jan. 1996.

[3] C. Puente, J. Romeu, R. Pous, and A. Cardama, "On the behavior of the Sierpinski multiband antenna," *IEEE Trans. Antennas Propagat.*, vol. 46, pp. 517–524, Apr. 1998.

[4] J. D. Kraus, *Antennas*, 2nd ed. New York: McGraw-Hill, 1988.

[5] R. F. Harrington, *Field Computation by Moment Methods*. New York: MacMillan, 1968.

On the Control of Edge Diffraction in Numerical Rough Surface Scattering Using Resistive Tapering

James C. West

***Abstract*—The use of resistive loading to remove edge effects in electromagnetic scattering from rough surfaces with finite conductivity has been considered. An electric field integral equation formulation using impedance boundary conditions was implemented to model the conductivity of sea water at X band. The resistive loading was added over surface sections within three wavelengths of the modeled edges. A resistive taper synthesized to control the sidelobe level in scattering from flat, perfectly conducting plates proved better able to reduce edge diffraction than a power-law taper of a type that is often used. The calculated scattering from test profiles that model breaking water waves using the resistive loading show good agreement with those found using a reference scattering approach provided that the local grazing angle on the loaded surface section is greater than 20°.**

***Index Terms*—Moment method, rough surfaces, sea surface electromagnetic scatter.**

I. INTRODUCTION

When using a moment-method based approach to numerically model the electromagnetic scattering from rough surfaces of unlimited extent, the primary limiting factor is that the modeled surface must be truncated so that the discretized integral equation will be treatable with finite computer resources. This truncation introduces artificial surface edges that, if left untreated, give nonphysical diffraction that can greatly affect the accuracy of the approach, both through direct back-diffraction and through interactions with the true surface features. Several methods have been introduced to reduce the edge effects. The most common approach is to apply a weighting function to the illumination that reduces it to negligible levels at the edges [1]. Unfortunately, the length of the modeled surfaces must be increased with decreasing grazing angles to give electromagnetically valid illumination, effectively limiting the approach to surfaces that are rough in only one dimension at the smallest grazing. Use of periodic boundary conditions [2] is similarly computationally prohibitive with two dimensional (2-D) rough surfaces, as is the synthesis of an equivalent radar pulse by repeating the analysis at multiple frequencies [3]. The hybrid approach extending the moment method with the geometrical theory of diffraction (MM/GTD) used in [4] is only applicable to 1-D rough surfaces.

Manuscript received April 1, 2002; revised November 27, 2002. This work was supported by the U.S. Office of Naval Research Ship Structures and Systems S&T Division under Grant N00014-00-1-0082 (Program Manager Dr. R. P. Radlinski).

The author is with the School of Electrical and Computer Engineering, Oklahoma State University, Stillwater, OK 74078 USA (e-mail: jwest@okstate.edu).

Digital Object Identifier 10.1109/TAP.2003.818775

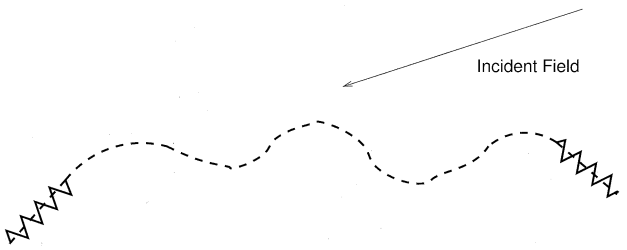

Fig. 1. Arbitrary rough surface with resistive loading added at the edges.

Using an alternative approach, Oh and Sarabandi [5] resistively loaded the ends of perfectly conducting rough surfaces and showed that edge effects were significantly reduced. This approach has the advantage that the additional computational expense of applying the loading is minimal. Here, the resistive loading of edges for rough surface scattering is further considered. Both the power-law resistive taper used by Oh and Sarabandi, as well as the taper introduced by Haupt and Liepa [6] for the control of sidelobes in scattering from perfectly conducting flat plates, are investigated. The scattering from deterministic surfaces that have features that are electromagnetically large is used as test cases, thereby giving a more complete test than the slightly rough surfaces used in [5]. Also, the loading is applied to surfaces that have finite (but large) conductivity.

II. APPROACH

Resistive loading is applied to the edges of an arbitrary rough surface as shown in Fig. 1. The resistive loading used by Oh and Sarabandi [5] is given by $R(x) = \eta_0(1 - x/L)^4$, where η_0 is the intrinsic impedance of free space, x is the distance from the surface end, and L is the total distance over which the loading is applied. This loading is hereafter referred to as the "power-law taper." Haupt and Liepa [6] synthesized a loading to give a surface current distribution across a perfectly conducting plate that approximates a Taylor antenna-aperture excitation, designed to control the sidelobe level in off-specular scattering from the plate. This loading is hereafter referred to as the "Taylor taper." Haupt and Liepa applied their taper across the full length of the surface. Here, the taper was separated at its center point and applied to the two edges of the modeled surface. The Taylor taper is given by [6]

$$R(Z) = \eta_0 \left\{ 2L \left[1 + 2 \sum_{n=1}^{\bar{n}-1} f(n) \cos\left(\frac{\pi n x}{L}\right) \right]^{-1} - \frac{1}{2} \right\} \quad (1)$$

where

$$f(n) = \begin{cases} \frac{[(\bar{n}-1)!]^2}{(\bar{n}-1+n)(\bar{n}-1-n)} \prod_{m=1}^{\bar{n}-1} \left(1 - \frac{n^2}{w_m^2}\right), & |n| < \bar{n} \\ 0, & |n| \geq \bar{n} \end{cases} \quad (2)$$

$$w_m = \begin{cases} \bar{n} \sqrt{\frac{A^2 + (m-0.5)^2}{A^2 + (\bar{n}-0.5)^2}}, & |n| < \bar{n} \\ n & |n| \geq \bar{n} \end{cases} \quad (3)$$

and $A = (1/\pi)\cosh^{-1}(10^{q/20})$. In this paper, the taper was synthesized with $\bar{n} = 9$ and $q = 90$. Ideally this would yield nine sidelobes